Sub- and super-shear ruptures during the 2023 *Mw* 7.8 and *Mw* 7.6 earthquake doublet in SE Türkiye

D. Melgar[1*], T. Taymaz[2], A. Ganas[3], B.W. Crowell[4], T. Öcalan[5], M. Kahraman[6], V. Tsironi [3,7], S. Yolsal-Çevikbilen[2], S. Valkaniotis [8], T.S. Irmak[9], T. Eken[2], C. Erman[2], B. Özkan[2], A.H. Doğan[5], C. Altuntaş[5]

[1] Department of Earth Sciences, University of Oregon, Eugene, U.S.A, dmelgarm@uoregon.edu
[2] Department of Geophysical Engineering, The Faculty of Mines, Istanbul Technical University, Maslak 34467, Sarıyer, Istanbul, Türkiye taymaz@itu.edu.tr, yolsalse@itu.edu.tr, eken@itu.edu.tr, ermanc@itu.edu.tr, ozkanber@itu.edu.tr
[3] National Observatory of Athens, Athens, Greece aganas@noa.gr , vtsironi@noa.gr
[4] Department of Earth and Space Sciences, University of Washington, Seattle, Washington crowellb@uw.edu
[5] Department of Geomatic Engineering, Faculty of Civil Engineering, Yildiz Technical University, Davutpaşa 34349, Istanbul, Türkiye tocalan@yildiz.edu.tr, alihasan@yildiz.edu.tr, cemali@yildiz.edu.tr

[6] Eurasia Institute of Earth Sciences, Istanbul Technical University, Maslak 34469, Sarıyer, Istanbul, Türkiye metinkahraman@itu.edu.tr
[7] Department of Geology, University of Patras, 26504 Rio, Greece
[8] Department of Civil Engineering, Democritus University of Thrace, 67100 Xanthi, Greece svalkani@civil.duth.gr
[9] Department of Geophysical Engineering, Kocaeli University, 41380 Umuttepe, Kocaeli, Türkiye irmakts@kocaeli.edu.tr

*Corresponding author: dmelgarm@uoregon.edu, @geosmx

This manuscript is undergoing peer review at Seismica. This is a non-peer reviewed preprint submitted to EarthArXiv

Author contributions

Conceptualization: D.M, T.T., A.G., B.C.
Data Curation: T.T., B.C., M.K., S.Y.C., T.Ö., C.E., B.Ö., A.H.D., C.A., V.T, S.V
Formal Analysis: D.M., T.T., M.K., B.C., A.G., V.T, S.V
Funding Acquisition: D.M, T.T., A.G., B.C.
Investigation: All authors
Methodology: D.M., T.T., B.C.
Project Administration: D.M, T.T., A.G., B.C., T.Ö.
Resources: D.M, T.T., A.G., B.C., T.Ö.
Software: D.M, T.T., M.K., A.G., B.C, S.Y.C., V.T, S.V
Supervision: D.M, T.T., A.G., B.C.
Validation: D.M., T.T., B.C.
Visualization: D.M., T.T.
Writing – original draft: D.M, T.T., A.G., B.C
Writing – review & editing: All authors

Abstract

An earthquake doublet (*Mw* 7.8 and *Mw* 7.6) occurred on the East Anatolian Fault Zone (EAFZ) on February 6th, 2023. The events produced significant ground motions and caused major impacts to

life and infrastructure throughout SE Türkiye and NW Syria. Here we show the results of earthquake relocations of the first 11 days of aftershocks and rupture models for both events inferred from the kinematic inversion of HR-GNSS and strong motion data considering a multi-fault, 3D geometry. We find that the first event nucleated on a previously unmapped fault before transitioning to the East Anatolian Fault (EAF) rupturing for ~ 350 km and that the second event ruptured the Sürgü fault for ~ 160 km. Maximum rupture speeds were estimated to be 3.2 km/s for the Mw 7.8 event. For the Mw 7.6 earthquake, we find super-shear rupture at 4.8 km/s westward but sub-shear eastward rupture at 2.8 km/s. Peak slip for both events were as large as ~8m and ~6m, respectively.

Second language abstract: Özet (Turkish)

6 Şubat 2023 tarihinde Doğu Anadolu Fay Zonu'nda (DAFZ) *Mw* 7.8 ve *Mw* 7.6 büyüklüklerinde bir deprem çifti meydana geldi. Depremlerin ürettiği kuvvetli yer hareketleri güneydoğu Türkiye ve kuzeybatı Suriye'de yaşam ve altyapı üzerinde önemli etkilere ve yıkımlara neden oldu. Bu çalışmada, deprem çifti için çoklu fay ve bütünleşik üç boyutlu (3B) fay geometrisi kullanarak HR-GNSS ve kuvvetli yer hareket verilerinin (SGM) birlikte analiz edildiği kinematik ters çözüm sonuçlarını göstermekteyiz. *Mw* 7.8 ve *Mw* 7.6 depremleri için yırtılma hızlarının sırasıyla 3.2 km/s ve 5.0 km/s yüksek-yırtılma hızı ve doğuya doğru 2.8 km/s düşük-yırtılma hızı davranışları gösterdiğini bulduk. Deprem çifti için maksimum yer değiştirme miktarları sırasıyla ~8m (M*w* 7.8) ve ~6m (M*w* 7.6) olarak hesaplanmıştır.

Third language abstract: Arabic

في 6 فبراير 2023. (EAFZ) على خط العيوب الأناضولي الشرقي (Mw 7.6 و Mw 7.8) حدث زلزال مزدوج أدت هذه الأحداث إلى حركات أرضية كبيرة وتسببت في آثار كبيرة على الحياة والبنية التحتية في جنوب شرق تركيا وشمال غرب سوريا. هنا نعرض نتائج إعادة مواقعة الزلازل المتتالية في الأيام الأولى من ما بعد الزلزال وعكس وحركة HR-GNSS الحركية لكل من الأحداث باستخدام هندسة ثلاثية الأبعاد متعددة الأخطاء والتي تستخدم بيانات قوية. نجد أن الحدث الأول نشأ على خط العيوب الذي لم يتم رصده سابقًا قبل الانتقال إلى العيب الأناضولي الشرقي بطول يصل إلى 350 كيلومترًا وأن الحدث الثاني قطع خط العيوب سورجو لمسافة تصل إلى 160 كيلومترًا. كانت نجد أن الانفجار تجاوز سرعة الصوت ، Mw 7.6 بالنسبة للزلزال .Mw 7.8 سرعة الانفجار القصوى 3.2 لحدث بمقدار 4.8 كم / ثانية نحو الغرب ولكن بسرعة الصوت بمقدار 2.8 كم / ثانية نحو الشرق. كانت الانزلاق الأقصى لكل من الأحداث حوالي 8 متر وحوالي 6 متر على التوالي.

Non-technical summary

Two very large earthquakes occurred in south-eastern Türkiye on February 6th 2023. In this paper we calculated kinematic models of how much the faults moved during both events and found very large motions of as much as 6-8 m. We further calculated how fast the faults broke and found a "normal" behavior for the magnitude 7.8 earthquake but also found that the magnitude 7.6 broke extremely quickly in one direction (west) but at normal speed in the other direction (east). This fact is scientifically interesting and important to understand the nature of why shaking was so strong in the region.

1. Overview of the events

On February 6th, 2023 at 01:17:35 UTC the *Mw* 7.8 Nurdağı-Pazarcık earthquake nucleated ~15km southeast of the mapped trace of the East Anatolian Fault Zone (EAFZ, Figure 1A). Relocations (Figures 1B,1C) place the hypocenter at (37.0234° E, 37.2444° N, h=12 km) and analyses of teleseismic data show a left-lateral source mechanism on a vertical or near vertical fault. A vigorous aftershock sequence followed and a little over 9 hours after the first event, at 10:24:49 UTC, the *Mw* 7.6 Ekinözü earthquake occurred with a hypocenter at (37.2756° E, 38.0900° N, h=15 km). It

locates close to the mapped trace of the Sürgü fault (SF), and, as the event is of large magnitude and on a separate structure, we consider it as part of a “doublet” rather than a traditional mainshock/aftershock sequence (see Taymaz et al. 2022).

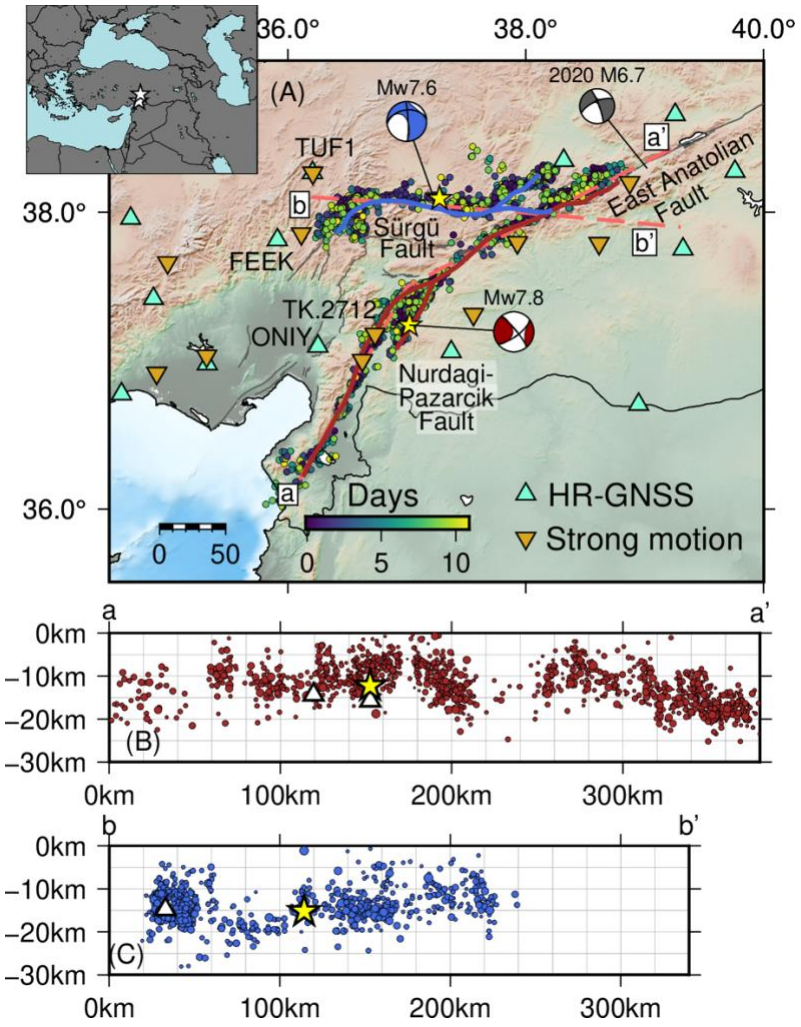

Figure 1. *(A) Simplified map of the study region showing the focal mechanisms for both events in the earthquake doublet. Known and mapped fault surface traces are shown as dark grey lines. The East Anatolian (EAF) fault and Sürgü fault (SF) are labeled. The inferred Nurdağı-Pazarcık Fault (NPF) is labeled as well. The thick red line denotes the surface trace of the geometry used for inversion of the Mw 7.8 event. The thick blue line is the surface trace of the geometry assumed for the Mw7.6 earthquake. The first 11 days of relocated aftershocks are shown. HR-GNSS and strong motion stations used in the inversions are depicted by triangles and inverted triangle respectively. The grey moment tensor is for the. M6.7 2020 Doğanyol-Sivrice earthquake. (B) Aftershock cross section across profile a-a'. (C) Aftershock cross section across profile b-b'. In both (B) and (C) stars are the doublet hypocenters and triangles denote events with Mw > 6.*

Ground motions recorded by a dense network of strong motion stations and inferred from the ShakeMap product show intensities as high as MMI 8 or 9 for both events (USGS 2023a,b). At the time of writing, reports in the news media indicate at least 45,000 fatalities and over 5 million displaced people in Türkiye and Syria. The two earthquakes represent the largest in the EAF

system and produced the largest ground motions in instrumental times. They have been catastrophic for the entire region.

The East Anatolian Fault Zone (EAFZ) is one of the most seismically active areas in Türkiye and the Middle East. The tectonics of the EAFZ are complex and are still being studied to fully understand the geologic history of the region. The EAFZ is part of a major fault zone that runs through eastern Türkiye as it accommodates the tectonic movement between the Arabian and Anatolian microplates (Ambraseys, 1989). This shear deformation zone is represented by a 580-km long plate boundary and is associated with frequent shallow seismicity in the top ~20-25 km of the crust (Taymaz et al., 1991; Tan and Taymaz, 2006; Melgar et al. 2020a; Taymaz et al. 2021). Relative plate motion is accommodated primarily by left-lateral strike-slip faulting at slip rates of 10±1 mm/yr (Reilinger et al., 2006) and has caused a series of destructive earthquakes in eastern Türkiye and northwest Syria as documented by historical records (Ambraseys and Jackson, 1998; Taymaz et al., 1991; Tan and Taymaz, 2006). Recent geological and geomorphic data indicate that the EAFZ has displaced the Euphrates River by 12 km since the mid-Quaternary (Trifonov et al. 2018) thus attaining a mean geological slip rate of 12-15 mm/yr. Yet, despite the dramatic effects of this fault's activity, a lack of high-resolution geodetic displacement data (e.g., achievable with continuous high-rate GNSS observations, HR-GNSS) has limited the capacity of constraining fault segmentation patterns, slip rate variations, earthquake recurrence intervals, and rupture dynamics.

Within this context, the earthquake doublet is of keen scientific interest for the region and for the study of large strike-slip systems generally. Here we will present the results of aftershock relocations and of kinematic slip inversions on a multi-fault 3D geometry using HR-GNSS and strong motion data. We will show that, for the *Mw* 7.8 the kinematics are complex – it nucleates on a previously unmapped structure and propagates to the EAF which then triggers and slip bilaterally with a maximum rupture speed of 3.2 km/s. Likewise the *Mw* 7.6 ruptures bilaterally on the curved Sürgü fault at super-shear speeds westward, likely as high as ~4.8 km/s, but sub-shear eastward at 2.8 km/s. The slip is then partitioned between a splay parallel to the EAF and the continuation of the SF to the intersection with the EAF.

2. Available Data and Methods

We used regional geodetic and seismological data to produce an aftershock catalog and slip model as follows.

2.1 Double-Difference Hypocenter Relocations

We produce relative locations for a total of 5077 earthquakes, including, the mainshocks of the doublet, and 9 large aftershocks with magnitudes between *Mw* 5.5 to 6.6. The data for this were acquired from the Disaster and Emergency Management Presidency of Türkiye (AFAD). It includes *P*- and *S*- phase arrivals from available stations selected by an automatized earthquake detection based on LTA/STA algorithm and initial locations estimated by the *Hypoinverse* algorithm (Klein, 2014). Most of the hypocentral depth estimates for these auto-located earthquakes range from 6.9 km to 7.1 km, i.e., more than 60% percent of aftershocks in this limited catalog.

To improve on this, we applied a relative earthquake location algorithm, *hypoD*D (Waldhauser and Ellsworth, 2000) using absolute *P*- and *S-wave* travel-time phase readings published in the AFAD bulletin. The algorithm makes use of earthquake pairs; with very small hypocentral differences compared to event to inter-station distances. This allows direct association of the spatial offsets between the pairs to time delays between two events observed at a single station (Waldhauser and Ellsworth, 2000). hypoDD minimizes the difference between observed and calculated travel time residuals using relative hypocenter locations and origin times for all observed event-station pairs

in an iterative manner. This overcomes potential bias originating from insufficient knowledge of structural complexities (e.g., velocity heterogeneities) along the source-receiver path, and, in this way, provides high-resolution hypocenter locations.

Travel-time differences are estimated for event pairs with less than 10 km of interevent distances and with a minimum of 8 links to define up to 10 neighbors at all 177 stations located within 200 km distance from the center of cluster. Initially 4756 out of 5077 aftershocks within the first 11 days were located following the Nurdağı-Pazarcık and Ekinözü earthquake doublet. Relative locations and origin times (OT) were obtained by a single set of 15 iterations in which large residuals were underestimated to suppress potential bias in the solution. We took a 1-D initial velocity model that was updated through the relocation process of the 24 January 2020 *Mw* 6.7 Doğanyol–Sivrice earthquake and its aftershock sequence (Melgar et al., 2020a; Taymaz et al., 2021). Our final database (see Data and Code Availability) consists of 2909 relocated events that had the highest resolution solutions (Figure 1A).

2.2 Source inversion

Given the complexity of the events, defining the 3D geometry for inversion (Figures 1,2) is critical to success of the modeling. We combined several sources of information to decide on the geometry as follows: We used the aftershocks, mapped traces of all known structures (EAFZ, and SF) and mapped surface ruptures from remote sensing (Reitman et al., 2023). We infer there is a structure, which we hence call the *Nurdağı-Pazarcık Fault* (NPF) offset from the main strand of the EAF. We used the general trend of the aftershocks and a small, mapped surface rupture to define its strike. As we will discuss later, this fault is necessary to fit the data. Further, the large (~15 km) offset between the hypocenter and the trace of the EAF necessitates it. For the junction of the SF with the EAF we used the mapped trace which connects the two faults. We also extended the SF into a small splay parallel to the EAF which is clearly visible in mapped surface offsets (Retiman et al., 2023). We used a vertical dip for the EAF southwest of the junction with the SF and used a vertical dip for the NPF as well. For the EAFZ northwest of the junction with the SF, and for the SF itself, we used a northward trending dip of 80°. This is supported by observations by Taymaz et al. (1991), Melgar et al. (2020a) and Taymaz et al. (2021) that reports a northward dipping geometry during the *Mw* 6.7 Doğanyol-Sivrice earthquake in the segment of the EAF immediately northeast of where rupture for the *Mw* 7.8 arrests. Additionally, the aftershocks are offset from the mapped surface traces and suggest a gentle northward deviation from vertical. We extended these geometries to a seismogenic depth of 20 km; this is supported by general observations of seismicity in the region from (Türkelli et al., 2003) and from the aftershocks (Figure 1B,C). The 3D surface is meshed using a finite element meshes into triangles of mean vertex length of ~5 km, this results in 482 subfault elements and 256 subfault elements for the *Mw* 7.8 and *Mw* 7.6, respectively.

Next, we processed the geodetic and geophysical data as follows. HR-GNSS solutions were calculated at 1 Hz sampling rate using the precise point positioning method (PPP) as implemented in GispyX (Bertiger et al., 2020). We used Jet Propulsion Laboratory rapid clocks and orbits and rotated the solutions from geodetic coordinates to topocentric north, east, and up (vertical) coordinates. The displacement waveforms were low-pass filtered to 0.4 Hz prior to inversion. Likewise, the strong motion data were processed by removing the instrument gain, removing the pre-event mean, and integrating to velocity for the *Mw* 7.6 and to displacement for the *Mw* 7.8. They were then bandpass filtered between 0.05 and 0.4 Hz, a total of 60 waveforms extracted from 12 three-component GNSS and 8 three-component strong motion sites contributed to the source inversion of the *Mw* 7.8 event. For the *Mw* 7.5 we used 10 three-component HR-GNSS and 5 three-component strong motion stations for a total of 45 waveforms.

For the kinematic inversion, we employed the open-source MudPy code (Melgar and Bock, 2015), which implements the linearized multi-time window method. Elastodynamic Green's functions for both data sets were computed using the frequency-wavenumber integration approach of Zhu and Rivera (2002). We assumed the 1-D layered model of Taymaz et al. (2021), which is appropriate for the region. The Green's functions (GFs) were filtered in the same passbands as the data before inversion. Rupture is allowed to nucleate at the hypocenter and a maximum rupture speed, v_r^{max}, is imposed. Note that in a multi-time window inversion this rupture speed is the upper bound allowed, slower rupture speeds are possible with subsequent time windows. We tested for both ruptures a range of values from 2.4 to 3.8 km/s for the *Mw* 7.8 and 2.0 to 6.0 km/s for the *Mw* 7.6 (Figure 2C).

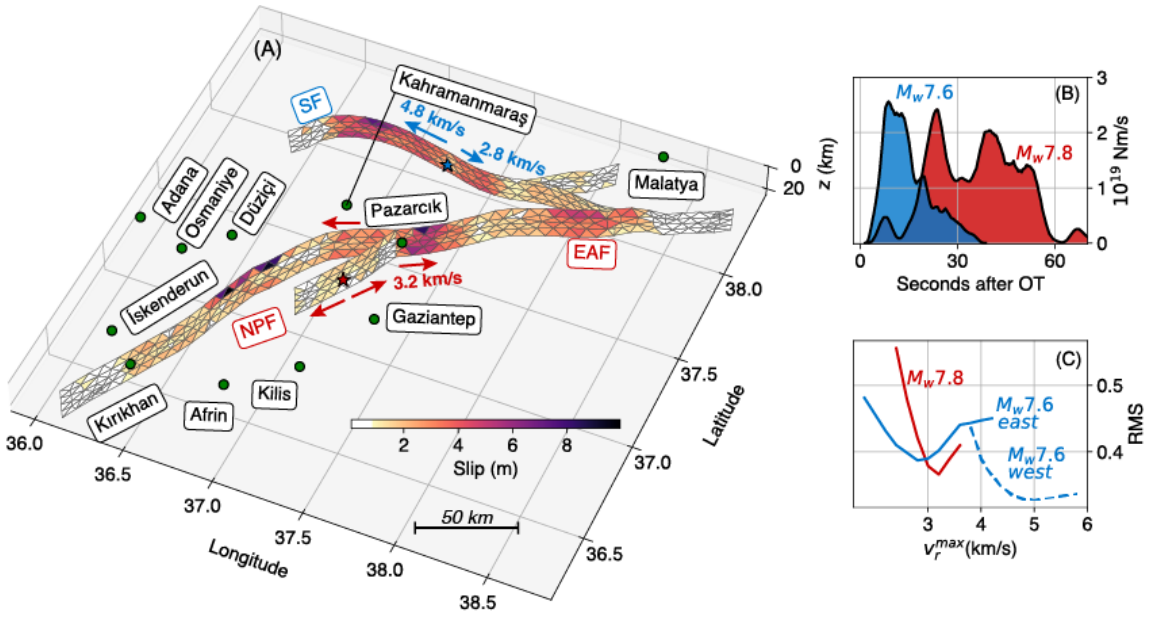

Figure 2. *(A) Perspective view of the assumed inversion geometry for both events. The Mw 7.8 ruptures on the EAF and NPF, the Mw 7.6 on the SF. Shown are the final best fitting slip distributions. Labeled in green circles are population centers in the region. (B) Source time functions for both ruptures. (C) RMS misfit as a function of maximum rupture speed v_r^{max} allowed in the inversion for both events. For the Mw 7.6 we distinguish between misfit for stations east or west of the hypocenter. Best fitting values are 3.2 km/s for the Mw 7.8 and 2.8 and 5.0 km/s for the Mw 7.6.*

Each subfault has a triangular slip rate function with fixed rise time, we used 5 s and 3 s for the *Mw* 7.8 and *Mw* 7.6 respectively. These values are obtained from the measurements of average rise times by Melgar and Hayes (2017) for large events worldwide. Individual subfaults are then allowed to slip on one of five time windows of this rise time, with each window overlaping 50% with the previous one. A non-negative least squares solver is used, and we restrict the rake vector for all subfaults to a 90° window between -45° and 45°. The inversion is stabilized using Tikhonov regularization; no smoothness constraint (e.g., such as a Laplacian) is imposed. The regularization parameter is chosen using the L-curve criterion. Each of the two types of data are weighted according to their individual L2 norms as explained in (Melgar et al., 2020a) and the vertical component of the HR-GNSS is down weighted by a factor of 3 to account for its higher noise levels (e.g., Melgar et al., 2020b).

3. Results and brief discussion

3.1 Mainshock hypocenters and aftershock relocations

A careful inspection of time sequence of aftershock activity reveals three large aftershocks ranging from *Mw* 6.4 to 6.6 that occurred within 18 minutes of the first main-shock with locations respectively southwest of it and a *Mw* 5.6 to northeast 46 minutes later. The second main-shock occurred 9 hours after the first on the roughly E-W oriented Sürgü fault and it had a *Mw* 5.9 aftershock after 10 hours on the western end of the same fault system (Figure 1B). Within the entire aftershock sequence, the spatial distribution of our event relocations indicates an elongated activity through southwestern segment of the EAFZ including epicenter of Nurdağı-Pazarcık earthquake and along the E-W oriented Sürgü fault following Ekinözü earthquake (Figure 1C). Our relocations for the two mainshocks show 12.3 km of hypocenter depth falling within the upper crust for the *Mw* 7.8 Nurdağı-Pazarcık earthquake whereas Ekinözü earthquake is deeper at 15.2 km corresponding to the mid-crustal depth range. The depth distribution of the relocated aftershocks suggests the entire crust between 2 km to 25 km underwent deformation, mainly along major fault zones.

3.2 Kinematics of the *Mw* 7.8 Nurdağı-Pazarcık earthquake

The event hypocenter is offset ~15km from the trace of the EAF, additionally, there is a distinct cloud of aftershocks offset for the EAF. It is not feasible to associate it to the EAF given the good confidence in the hypocenter's location, and indeed, inversions that assume this have very poor fits to the data. We infer thus that a secondary structure, the NPF, hosts the rupture initiation.

Consider Figure 3 where we show HR-GNSS site ONIY and strong motion site TK.2712 which are located 68 and 79 km away from the hypocenter (Figure 1). Here from these time-series, we find that there are clearly two stages of ground motion. This must be considered during the kinematic inversion. Thus, we tested two scenarios for how rupture transfers from the NPF to the EAF. First, we allowed rupture on the EAF that starts at a time equivalent to the moment when *S*-waves from the NPF reach it. In this case, the fits to the GNSS and strong motion were poor, particularly with regard to the early stages of the waveforms, which were hard to model (e.g., Figures 3, 4). In a second scenario, we delayed the onset of slip on the EAF until the time the rupture front originating at the NPF reaches the intersection of the two faults. Here we finally see the fits to the data improve significantly (Figure 4). Snapshots of rupture propagation (Figure 5) and an animation of it (Supplementary S1, see Data and code availability) show that once the rupture reaches the EAF, at ~10s after origin time, it spreads bilaterally across the fault. Slip rates reach as high as 1.5 m/s in the model, the total length of rupture on the EAF is ~350 km and peak slip is 9 m – this yields a final moment of $M_0 = 6.51 \times 10^{20}$ N-m (*Mw* 7.8). The apparent complexity of the source time function is identified by many peaks reflecting the interaction of these two faults (Figure 2B). Finally, we find that fits to the data are highest for $v_r^{max} = 3.2$ km/s which corresponds to about ~90% of shear wave speed at the depths where most of the slip takes place.

3.3 Kinematics of the *Mw* 7.6 Ekinözü earthquake

For the *Mw* 7.6 rupture nucleates on the SF and spreads bilaterally (Figure 5) and has muted slip at both ends of the fault (Figure 2A). The event has high peak slip, ~7m and the total length of rupture is ~160 km. Fits to the waveforms are also good (Figure 6) and have similar RMS (Figure 2C) although there are later arrivals at strong motion sites TK.0205, and TK.4404 that cannot be modeled smoothly. These could reflect path or site-specific conditions that lead to amplifications that cannot be explained within our simple 1D approach. Nonetheless, the fits are good and the final model (shown in Figure 2) has a seismic moment of $M_0 = 3.64 \times 10^{20}$N-m (*Mw* 7.6). The most interesting aspect of this event is that the joint modeling of HR-GNSS and strong motion required

two different v_r^{max} values in order to fit the data (Figure 2C). We tried several values of a single v_r^{max} and quickly noticed that stations east or west of the rupture prefer different values (Figure 2C). There is a broad plateau of low RMS between 4.6 and 5.4 km/s for sites west of the rupture. As an example, stations TUF1 and FEEK (locations in Figure 1A) cannot be explained by sub-shear speeds. This preferred v_r^{max} is much larger than the ~3.7 km/s shear wave speed at the depths where most of the slip takes place. This is compelling evidence that the event had super-shear rupture to the west. Interestingly the sites to the east display high misfits when v_r^{max} is high and prefer much lower values closer to ~2.8 km/s. For our best-fitting model (Figure 2A,6) we imposed a combination of super-shear to the west and sub-shear to the east. This can be seen clearly in Animation S1 as well.

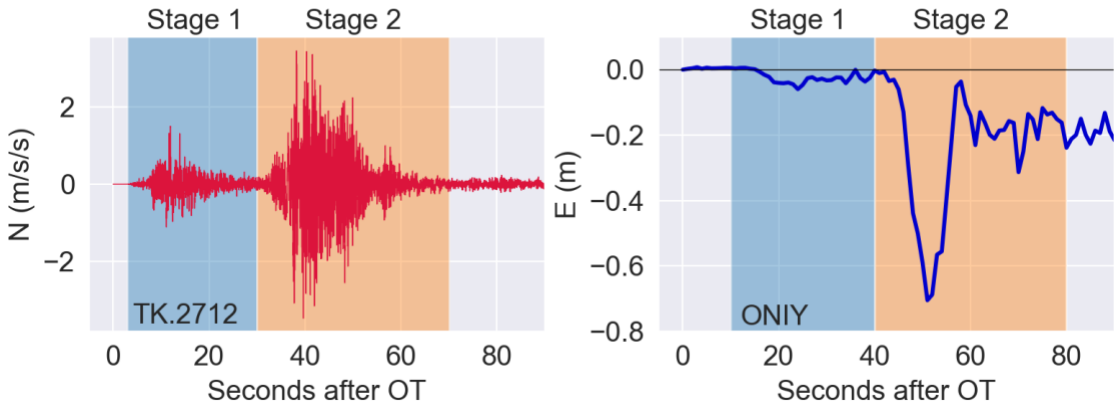

Figure 3. *North component of strong motion station TK.2712 and east component of HR-GNSS site ONIY (see Figure 1 for locations). For each waveform we have labeled what clearly appears as two distinct stages of ground motion. Our tests showed that fitting the early stage 1 of the waveforms requires rupture on a structure, the NPF, separate from the EAF.*

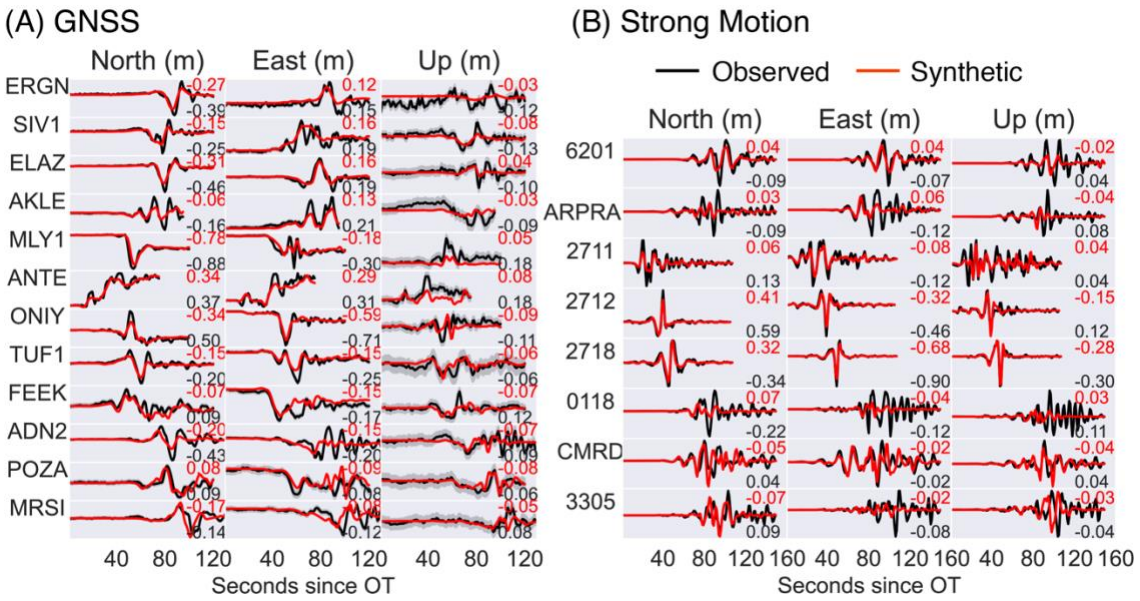

Figure 4. *Fits to the HR-GNSS (A) and strong motion (B) for the best fitting Mw 7.8 model. Black is the observed and red the modeled waveforms. Inset numbers show the peak amplitudes for each waveform.*

3.4 Discussion and outstanding questions

The results shown here are a brief "first-look" analysis into two complex events and point to several important open questions, which will warrant further investigation. The *Mw* 7.8 earthquake ruptured the southern three segments of the EAFZ which last broke in 1513, 1872, and 1893 (see Taymaz et al., 2021 for a summary) and arrested at the source zone of the recent 2020 *Mw* 6.7 Doğanyol-Sivrice earthquake (e.g. Melgar et al., 2020a). Meanwhile the *Mw* 7.6 likely broke the entire Sürgü fault which had not had a significant earthquake since 1544 (Taymaz et al., 2021). Understanding the timing, stress interactions between these events and further implications for other neighboring structures will be important.

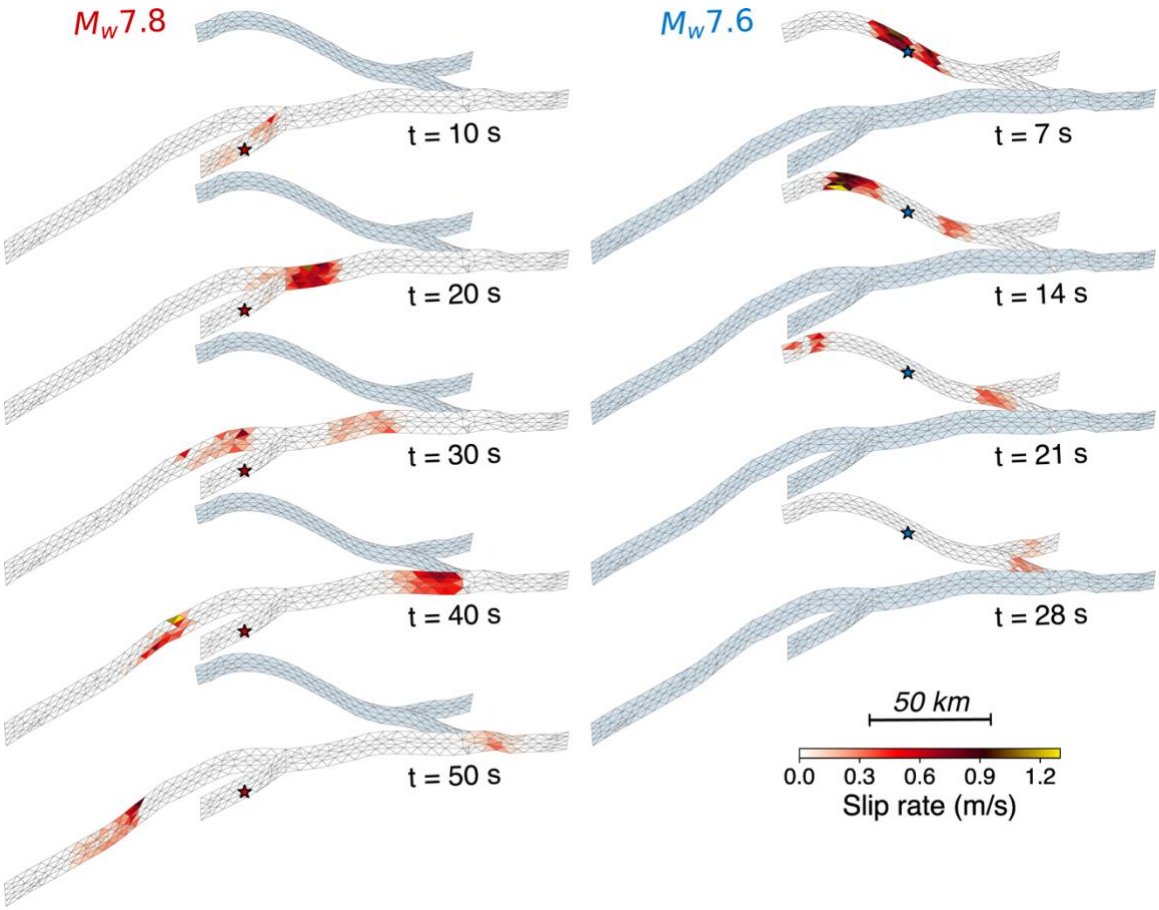

Figure 5. *Snapshots of rupture propagation for both events. Plotted is slip rate on each subfault at specified instants in time.*

Regarding the ruptures, the strong evidence provided by the near-field HR-GNSS and strong motion data supports the conclusion that the second event involved a super-shear rupture, based on the relatively high estimate of v_r^{max}. The rapid finite-fault model published by the U.S. Geological Survey (USGS, 2023b) similarly shows zones of super-shear rupture. Our preferred westward v_r^{max} of 4.8 km/s is very high but has been seen before in other super-shear strike slip events such as during the 1999 *Mw* 7.4 Izmit, 2004 *Mw* 7.8 Denali, 2013 *Mw* 7.5 Craig, Alaska and other earthquakes (Bouchon et al., 2001, Frankel., 2004, Yue et al., 2013). Additionally, we notice again that this is the maximum allowed speed, slower speeds are possible with the multi-time window approach and indeed, in Figure 5, we observe that to the east the initial stage of rupture has very modest slip rates and the slower rupture speeds correspond to larger slip rates. The area where

stations TUF1 and FEEK are located, towards the west, is where the slip pulse exhibits significant slip at v_r^{max}. Understanding the contributions of these kinematics to ground motion will be of great importance. Finally, a remaining open question is why there is no obvious super-shear rupture in the first event. There, rupture seems to prefer propagation right at Rayleigh wave speeds and, while increasing v_r^{max} to slightly above shear-wave speed still produces low RMS the result is not nearly as obvious or dramatic as for the *Mw* 7.6 earthquake.

At a more granular level, a few structural questions remain as well. What is the exact nature of the NPF and how frequently does it participate in significant events? Additionally, the intersection of the SF and the EAF is structurally complex, mapped traces and the aftershocks hint at a secondary structure, sub-parallel to the EAF and immediately north of the SF. We find that rupture also branched out onto this structure. Here, remote sensing observations of crustal deformation will hold important clues. Using these data will not be without its challenges, as most observations, from InSAR for example, will have captured both events and many, if not all, the large aftershock. Separating the contributions to crustal deformation from individual events has been done for other similarly complex earthquake sequences (e.g., Goldberg et al., 2020) but it will require significant effort.

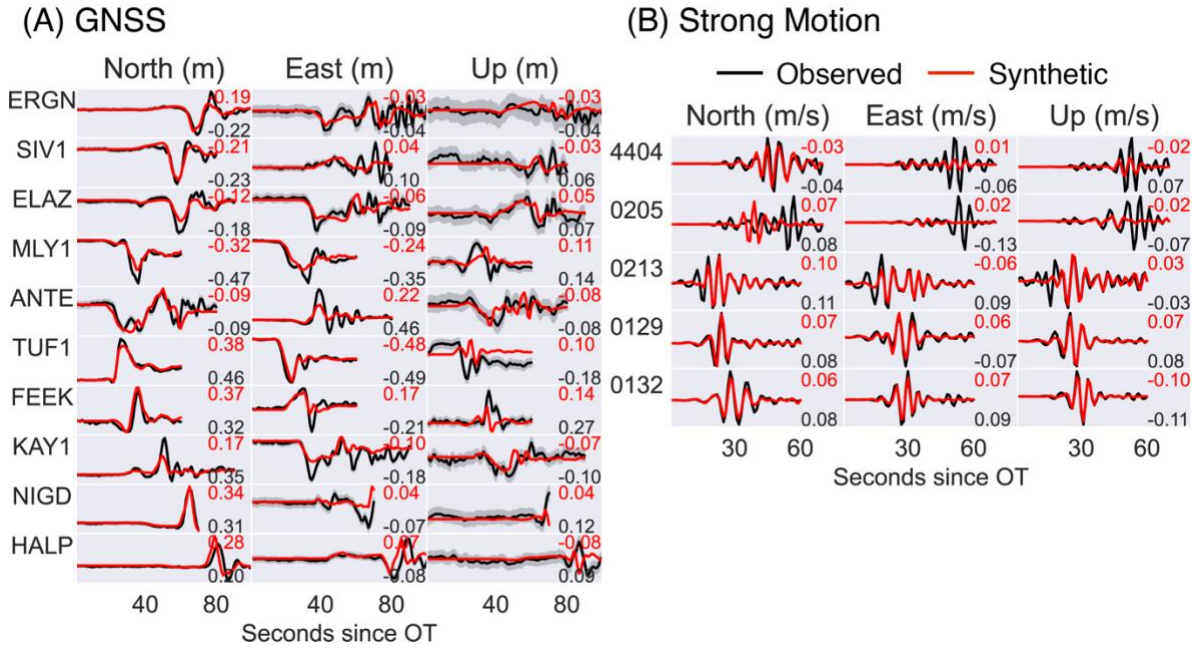

Figure 6. *Fits to the HR-GNSS (A) and strong motion (B) for the best fitting Mw 7.6 model. Black is the observed and red the modeled waveforms. Inset numbers show the peak amplitudes for each waveform.*

4. Conclusions

Here we have shown kinematic rupture models from joint inversion of HR-GNSS and strong motion data-sets and relocated aftershocks for the two events in the 2023 SE Türkiye earthquake doublet. We have used a complex multi-fault 3D geometry for inversion. We find that rupture speed is very close at the sub- to super-shear transition for the *Mw* 7.8 event and that it is super-shear for the westward rupture of the *Mw* 7.6 earthquake but sub-shear to the east. Peak slip exceeds 8m for both events and slip rates as high as ~1.5m/s are pervasive throughout. Rupture lengths where ~350 km for the Mw 7.8 event and ~160 km for the Mw 7.6 earthquake.

Acknowledgements

Strong motion data were retrieved from Department of Earthquake, Disaster and Emergency Management Authority of Türkiye (AFAD, Ankara) through Turkish National Strong Motion Network (https://doi.org/10.7914/SN/TK), and Kandilli Observatory and Earthquake Engineering Research Institute of Boğaziçi University (KOERI, Istanbul), last accessed on 18 February 2023. The contributors thank the CORS-TR (TUSAGA-Aktif-Türkiye) GNSS network administrated by General Directorate of Land Registry and Cadastre (TKGM) and General Directorate of Mapping (HGM) for releasing GNSS data. Tuncay Taymaz thanks to Istanbul Technical University Research Fund, Turkish Academy of Sciences (TÜBA) in the framework for Young Scientist Award Program (TÜBA-GEBİP), and the Alexander von Humboldt Foundation Research Fellowship Award for financial support and for further providing computing facilities and other relevant computational resources through Humboldt-Stiftung Follow-Up Program. We have further benefited from fruitful discussions with Tamer Y. Duman and Selim Özalp for interpretation of active neotectonics features observed in the region, with Ercan Yüksel and Oğuz C. Çelik for structural damages in the catastrophic area, and with D. Goldberg for the kinematic modeling.

Data and code availability

The hypoDD earthquake relocation code is freely available from the developers at https://www.ldeo.columbia.edu/~felixw/hypoDD.html. The MudPy slip inversion code is available on GitHub at https://github.com/dmelgarm/MudPy and a snapshot of the code can be found on Zenodo at Melgar et al. (2021). Data and models produced in this paper can be found at *zendo url here* – this includes the catalog of relocated events, waveforms and station locations used for inversion, 3D geometry definitions of the fault, and the final best fitting rupture models. GNSS solutions were processed with JPL's GipsyX software package, licensed to BWC at University of Washington.

Competing interests

The authors declare that they have no competing interests.

References

Ambraseys, N.N. (1989). Temporary seismic quiescence: SE Turkey, Geophys. J. Int. 96(2), 11–331, https://doi.org/10.1111/j.1365-246X.1989.tb04453.x

Ambraseys, N.N., Jackson, J.A. (1998). Faulting associated with historical and recent earthquakes in the Eastern Mediterranean region. Geophys. J. Int. 133, 390–406, https://doi.org/10.1046/j.1365-246X.1998.00508.x

Bertiger, W., Bar-Sever, Y., Dorsey, A., Haines, B., Harvey, N., Hemberger, D., ... & Willis, P. (2020). GipsyX/RTGx, a new tool set for space geodetic operations and research. Advances in space research, 66(3), 469-489.

Bouchon, M., Bouin, M. P., Karabulut, H., Toksöz, M. N., Dietrich, M., & Rosakis, A. J. (2001). How fast is rupture during an earthquake? New insights from the 1999 Turkey earthquakes. *Geophysical Research Letters*, *28*(14), 2723-2726.

Frankel, A. (2004). Rupture process of the M 7.8 Denali Fault, Alaska, earthquake: Subevents, directivity, and scaling of high-frequency ground motions. Bulletin of the Seismological Society of America, 94(6B), S234–S255. https://doi.org/10.1785/0120040612

Goldberg, D. E., Melgar, D., Sahakian, V. J., Thomas, A. M., Xu, X., Crowell, B. W., & Geng, J. (2020). Complex rupture of an immature fault zone: A simultaneous kinematic model of the 2019

Ridgecrest, CA earthquakes. *Geophysical Research Letters*, *47*(3), e2019GL086382. https://doi.org/10.1029/2019GL086382

Klein, F. (2014). User's Guide to HYPOINVERSE-2000, a Fortran Program to Solve for Earthquake Locations and Magnitudes, Open File Report 02-171 revised Version 1.40, June 2014.

Melgar, D., & Bock, Y. (2015). Kinematic earthquake source inversion and tsunami runup prediction with regional geophysical data: *Journal of Geophysical Research: Solid Earth*, *120*(5), 3324–3349. https://doi.org/10.1002/2014JB011832

Melgar, D., & Hayes, G. P. (2017). Systematic Observations of the Slip Pulse Properties of Large Earthquake Ruptures. Geophysical Research Letters, 44(19), 9691–9698. https://doi.org/10.1002/2017GL074916

Melgar, D., Ganas, A., Taymaz, T., Valkaniotis, S., Crowell, B. W., Kapetanidis, V., Tsironi, V., Yolsal-Çevikbilen, S., & Öcalan, T. (2020a). Rupture kinematics of 2020 January 24 *Mw* 6.7 Doğanyol-Sivrice, Turkey earthquake on the East Anatolian Fault Zone imaged by space geodesy. *Geophysical Journal International*, *223*(2), 862–874. https://doi.org/10.1093/gji/ggaa345

Melgar, D., Crowell, B. W., Melbourne, T. I., Szeliga, W., Santillan, M., & Scrivner, C. (2020b). Noise Characteristics of Operational Real-Time High-Rate GNSS Positions in a Large Aperture Network. *Journal of Geophysical Research: Solid Earth*, *125*(7). https://doi.org/10.1029/2019JB019197

Melgar, D. et al. (2021). dmelgarm/MudPy: v1.3. Zenodo. https://doi.org/10.5281/zenodo.5397091

Reilinger, R. et al. (2006). GPS constraints on continental deformation in the Africa–Arabia–Eurasia continental collision zone and implications for the dynamics of plate interactions. J. Geophys. Res., 111, B05411, https://doi.org/10.1029/2005JB004051

Reitman, N.G., Briggs, R.W, Barnhart, W.D., Thompson, J.A., DuRoss, C.B., Hatem, A.E., Gold, R.D., Mejstrik, J.D. (2023) *Preliminary fault rupture mapping of the 2023 M7.8 and M7.5 Türkiye Earthquakes.* DOI: https://doi.org/10.5066/P985I7U2

Tan, O., Taymaz, T. (2006). Active Tectonics of the Caucasus: Earthquake Source Mechanisms and Rupture Histories Obtained from Inversion of Teleseismic Body-Waveforms. In: Post-Collisional Tectonics and Magmatism in the Mediterranean Region and Asia, Geological Society of America, Special Paper 409, pp: 531-578, https://doi.org/10.1130/2006.2409(25)

Taymaz, T., Ganas, A., Berberian, M., Eken, T., Irmak, T.S., Kapetanidis, V., Yolsal-Çevikbilen, S., Erman, C., Keleş, D., Esmaeili, C., Tsironi, V., Özkan, B. (2022). The 23 February 2020 Qotur-Ravian Earthquake Doublet at the Iranian-Turkish Border: Seismological and InSAR Evidence for Escape Tectonics, Tectonophysics, Vol. 838, TECTO15364-229482, https://doi.org/10.1016/j.tecto.2022.229482

Taymaz, T., Ganas, A., Yolsal-Çevikbilen, S., Vera, F., Eken, T., Erman, C., Keleş, D., Kapetanidis, V., Valkaniotis, S., Karasante, I., Tsironi, V., Gaebler, P., Melgar, D., Ocalan, T. (2021). Source Mechanism and Rupture Process of the 24 January 2020 *Mw* 6.7 Doğanyol-Sivrice Earthquake obtained from Seismological Waveform Analysis and Space Geodetic Observations on the East Anatolian Fault Zone (Turkey), Tectonophysics, Vol. 804, TECTO14240-228745, https://doi.org/10.1016/j.tecto.2021.228745

Taymaz, T., Eyidoğan, H., & Jackson, J.A. (1991). Source Parameters of large earthquakes in the East Anatolian Fault Zone (Turkey), Geophysical Journal International, 106, 537-550, https://doi.org/10.1111/j.1365-246X.1991.tb06328.x

Trifonov, V.G., Çelik, H., Simakova, A.N., Bachmanov, D.M., Frolov, P.D., Trikhunkov, Y.I., Tesakov, A.S., Titov, V.M., Lebedev, V.A., Ozherelyev, D.V., Latyshev, A.V., Sychevskaya, E.K., (2018). Pliocene – Early Pleistocene history of the Euphrates valley applied to Late Cenozoic environment of the northern Arabian Plate and its surrounding, eastern Turkey. Quaternary International 493, 137-165, https://doi.org/10.1016/j.quaint.2018.06.009

Türkelli, N., Sandvol, E., Zor, E., Gok, R., Bekler, T., Al-Lazki, A., Karabulut, H., Kuleli, S., Eken,T., Gurbuz, C., Bayraktutan, S., Seber, D. and Barazangi, M. (2003). Seismogenic Zones in Eastern Turkey. Geophysical Research Letters, 30 (24), 8039, https://doi.org/10.1029/2003GL018023

U.S. Geological Survey (2023a). Event page for the M 7.8 - Central Turkey, earthquake, https://earthquake.usgs.gov/earthquakes/eventpage/us6000jllz/, last consulted February 20th, 2023

U.S. Geological Survey (2023b). Event page for the M 7.5 - 4 km SSE of Ekinözü, Turkey, earthquake, https://earthquake.usgs.gov/earthquakes/eventpage/us6000jlqa/, last consulted February 20th, 2023

Waldhauser, F., Ellsworth, W.L. (2000). A Double-difference Earthquake location algorithm: Method and application to the Northern Hayward Fault, California. Bull. Seismol. Soc. Am. 90, 1353–1368. https://doi.org/10.1785/0120000006

Yue, H., Lay, T., Freymueller, J. T., Ding, K., Rivera, L., Ruppert, N. A., & Koper, K. D. (2013). Supershear rupture of the 5 January 2013 Craig, Alaska (MW 7.5) earthquake. *Journal of Geophysical Research: Solid Earth*, *118*(11), 5903-5919.

Zhu, L., & Rivera, L. A. (2002). A note on the dynamic and static displacements from a point source in multilayered media: A note on the dynamic and static displacements from a point source. Geophysical Journal International, 148(3), 619–627. https://doi.org/10.1046/j.1365-246X.2002.01610.x